

NFN - Nationales Forschungsnetzwerk

Geometry + Simulation

<http://www.gs.jku.at>



Arc Fibrations of Planar Domains

Bert Jüttler, Sofia Maroscheck,
Myung-Soo Kim, Q Youn Hong

G+S Report No. 80

March 2019

FWF

Der Wissenschaftsfonds.

JKU
JOHANNES KEPLER
UNIVERSITY LINZ

Arc Fibrations of Planar Domains

Bert Jüttler^{a,*}, Sofia Maroscheck^a, Myung-Soo Kim^b, Q Youn Hong^b

^a*Institute of Applied Geometry, Johannes Kepler University, Linz/Austria*

^b*School of Computer Science and Engineering, Seoul National University, South Korea*

Abstract

It is well known that star-shaped domains possess particularly simple polar parameterizations, which are formed by the line segments that connect a suitably chosen center with the points on the domain's boundary. The polar parameterization is valid (i.e., regular everywhere except for the center) if the center is located in the kernel of the domain. In the case of a domain with a smooth free-form boundary curve, the kernel is a convex region which is enclosed by the curve and (some of) the boundary's inflection tangents. These parameterizations possess numerous applications, most recently also including domain parameterization in isogeometric analysis.

Since the class of star-shaped domains is quite limited, we propose to increase the flexibility of the underlying polar parameterizations by considering circular arcs that connect the center with the points on the domain's boundary. Parameterizations that are regular everywhere except at the center are said to form an arc fibration of a planar domain. We analyze the existence of an arc fibration with a given center and present an algorithm that computes it in the affirmative case. In addition, we explore the arc fibration kernel that contains the suitable center points.

Keywords: circular arcs, arc fibration, star-shaped, domain parameterization, isogeometric analysis

1. Introduction

The notion of *starshapedness*, which describes the property that a domain possesses at least one center point that sees every point on the domain's boundary, plays a fundamental role in numerous applications. It motivates the definition of the *kernel* of a domain, which is the set of all the possible center points.

The case of planar polygons was analyzed in the classical literature on Computational Geometry. Lee and Preparata (1979) proposed an algorithm that computes the kernel of a planar polygon (which is simply the intersection of all half-planes defined by the polygon's edges) with linear complexity. An efficient algorithm for the decomposition of polygons into star-shaped polygons was presented by Avis and Toussaint (1981), and it was shown that the problem of finding the minimum decomposition is NP hard (O'Rourke and Supowit, 1983).

These results have been extended to planar domains with free-form boundaries. Dobkin and Souvaine (1990) extended results from classical computational geometry to two- and three-dimensional domains, which are bounded by spline curves and surfaces (splinegons and splinehedrons). More recently, the visibility locations for planar domains bounded by closed smooth curves were investigated by Joshi et al. (2017). These locations generalize the notion of the center to non-star-shaped domains. This work is related to earlier results on visibility charts for continuous curves in the plane by Elber et al. (2005). These charts allow to analyze the visibility of the curve from a one-parameter set of candidate viewpoints, which may be interior or exterior to the object. Only very few contributions exist for domains in three-dimensional

*Corresponding author

Email addresses: bert.juettler@jku.at (Bert Jüttler), sofia.maroscheck@jku.at (Sofia Maroscheck), mskim@snu.ac.kr (Myung-Soo Kim), qhong@3map.snu.ac.kr (Q Youn Hong)

space. [Elber et al. \(2006\)](#) proposed algorithms for computing the kernel of a closed freeform rational surface, based on a plane-point duality. Besides segments of the original surface, the boundary surface of the kernel contains developable surface patches and even planar surface patches.

Our interest in star-shaped domains grew out of applications to numerical simulation within the framework of isogeometric analysis. The scaled boundary finite element method employs a polar parameterization of star-shaped domains via line segments, in order to derive a discretization of a partial differential equation. This method has recently been applied to domains given by a NURBS boundary representation ([Natarajan et al., 2015](#); [Chen et al., 2016](#)) in agreement with the isogeometric paradigm of exact geometry representation ([Hughes et al., 2005](#)).

In order to increase the flexibility of the polar parameterizations by line segments, which are available for star-shaped domains only, we propose to employ circular arcs that connect the center with the points on the domain’s boundary. Polar parameterizations of this type, which are regular everywhere except at the center, are said to form an *arc fibration* of a planar domain.

The choice of circular arcs is motivated by the well-established fact – which has been explored in Computational Geometry ([Aichholzer et al., 2011](#)) – that these curves form the natural generalization of line segments. Consequently, we will be able to analyze the existence of an arc fibration with a given center via certain geometric arguments, and to derive an algorithm that computes it in the affirmative case. These results will be presented in Sections 3, 4 and 5.

In addition, we will explore in Section 6 the *arc fibration kernel* of a domain, which is formed by the set of suitable center points. Finally we will summarize the paper and present some directions for further research.

2. Polar parameterizations

Throughout this paper we consider a simply connected planar domain $D \subset \mathbb{R}^2$. Its boundary ∂D is represented by a closed parametric curve

$$\mathbf{c}(t) = (x(t), y(t)), \quad t \in \mathbb{R},$$

with positive (i.e., counterclockwise) orientation. The curve is described by 1-periodic coordinate functions, $\mathbf{c}(t) = \mathbf{c}(t + 1)$, which are assumed to be C^2 -smooth.

We assume that the domain D contains the origin $\mathbf{0} = (0, 0)$. In this situation, it is possible to extend the parametric curve to a polar parameterization

$$\mathbf{p}(s, t), \quad s \in [0, 1], \quad t \in \mathbb{R}, \quad (1)$$

that satisfies

$$\mathbf{p}(0, t) = (0, 0), \quad \mathbf{p}(1, t) = \mathbf{c}(t) \quad \text{and} \quad \mathbf{p}(s, t) = \mathbf{p}(s, t + 1). \quad (2)$$

The parameter lines $t = \text{constant}$ connect the origin $\mathbf{0}$, which is called the *center* of the polar parameterization, with the boundary point $\mathbf{c}(t)$.

Parameterizations by lines are the simplest instances of polar parameterizations. These are obtained by performing linear interpolation of the origin and the boundary points,

$$\mathbf{p}(s, t) = (1 - s)\mathbf{0} + s\mathbf{c}(t) = (sx(t), sy(t)), \quad (3)$$

see Fig. 1. These parameterizations are regular (except for the singularity at the center) if and only if the domain is star-shaped with respect to the origin, which is characterized by the inequality

$$\det \begin{pmatrix} x(t) & x'(t) \\ y(t) & y'(t) \end{pmatrix} > 0 \quad \forall t \in \mathbb{R}.$$

More generally, a domain is said to be star-shaped if it satisfies this condition for a suitable choice of the coordinate system. The *kernel* of a domain is formed by all possible locations of the origin such that the

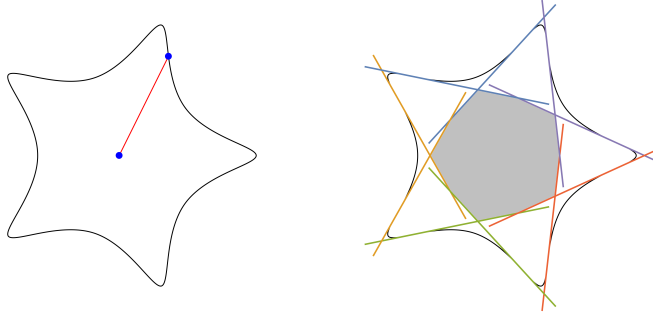


Figure 1: A star-shaped domain with a parameter line (left) of the polar parameterization and its kernel (right).

above condition is satisfied. It is a convex region which is bounded by the curve and by the tangents at the curve's inflection points, see again Fig. 1.

Clearly, the set of star-shaped domains is quite restricted. We improve the flexibility of polar parameterizations by considering circular arcs instead of straight line segments. These arcs form a slightly more general class of parameter lines.

3. Arc fibrations

Arc fibrations are a special class of polar parameterizations. We represent them by parameterizations of the form

$$\mathbf{p}(s, t) = \frac{(1-s)^2\nu_0(t)\mathbf{b}_0(t) + 2s(1-s)\nu_1(t)\mathbf{b}_1(t) + s^2\nu_2(t)\mathbf{b}_2(t)}{(1-s)^2\nu_0(t) + 2s(1-s)\nu_1(t) + s^2\nu_2(t)}, \quad (4)$$

which we construct with the help of a result of Zubé (2006) about the representation of circular arcs as rational linear Bézier curves with complex control points and weights, see Remark 1 below.

More precisely, the parameter lines $t = \text{constant}$ are circular arcs, which are described by rational Bézier curves of degree 2 (obtained from rational linear Bézier curves with complex control points and weights) with control points

$$\mathbf{b}_0(t) = \begin{pmatrix} 0 \\ 0 \end{pmatrix}, \quad \mathbf{b}_1(t) = \frac{x(t)^2 + y(t)^2}{2(x(t)\cos\varphi(t) + y(t)\sin\varphi(t))} \begin{pmatrix} \cos\varphi(t) \\ \sin\varphi(t) \end{pmatrix}, \quad \mathbf{b}_2(t) = \begin{pmatrix} x(t) \\ y(t) \end{pmatrix}.$$

and associated weights

$$\nu_0(t) = x(t)^2 + y(t)^2, \quad \nu_1(t) = x(t)\cos\varphi(t) + y(t)\sin\varphi(t), \quad \nu_2(t) = 1.$$

Obviously, the polar parameterization (4) satisfies (2) if the chosen function $\varphi(t)$ obeys the functional equation $f(\xi + q) = f(\xi) + C$, which characterizes *arithmetic quasiperiodic functions*, for the quasiperiod $q = 1$ and the constant $C = 2\pi$. Moreover, it can be confirmed by a short computation that the angle $\varphi(t)$ specifies the tangent direction

$$\left(\frac{\partial}{\partial s}\mathbf{p}\right)(0, t) = \begin{pmatrix} \cos\varphi(t) \\ \sin\varphi(t) \end{pmatrix} = \mathbf{v}(t) \quad (5)$$

at the center point. Finally we note that the denominator has a real root $s \in [0, 1]$ if and only if

$$\langle \mathbf{c}(t), \begin{pmatrix} \cos\varphi(t) \\ \sin\varphi(t) \end{pmatrix} \rangle = \nu_1(t) \leq -\sqrt{\nu_0(t)\nu_2(t)} = -\|\mathbf{c}(t)\|. \quad (6)$$

The polar parameterization is therefore well defined for all $s \in [0, 1]$ unless the vectors $\mathbf{c}(t) = (x(t), y(t))^T$ and $(\cos\varphi(t), \sin\varphi(t))^T$ are anti-parallel, i.e., provided that

$$\varphi(t) \notin \pi + \arg(x(t) + iy(t)), \quad (7)$$

where \arg denotes the argument¹ of a complex number and i is the imaginary unit.

Remark 1. As observed by Zubé (2006), the use of complex numbers is very convenient when working with rational parameterizations of circular arcs. In particular, he noted that rational linear Bézier curves with complex weights (which can equivalently be represented as rational quadratic Bézier curves) represent circular arcs. In fact, the curves $t = \text{constant}$ in (4) are equivalent to the rational linear curves

$$p_1(s, t) + ip_2(s, t) = \frac{(1-s) \frac{x(t)+iy(t)}{\cos \varphi(t)+i \sin \varphi(t)} (0+i0) + s \cdot 1 \cdot (x(t)+iy(t))}{(1-s) \frac{x(t)+iy(t)}{\cos \varphi(t)+i \sin \varphi(t)} + s \cdot 1}$$

where we identified points with complex numbers. \diamond

Now we introduce the central notion of this paper.

Definition 1. The polar parameterization (4), which is defined by the 1-periodic boundary curve $\mathbf{c}(t)$ and the 1-quasiperiodic function $\varphi(t)$ with shift 2π , is called an *arc fibration* if it is regular for all $(s, t) \in (0, 1] \times \mathbb{R}$.

Example 1 (Hourglass). We consider the 1-periodic cubic spline curve $\mathbf{c}(t)$ with uniform knots and control points

$$\begin{pmatrix} -75 \\ -373 \end{pmatrix}, \begin{pmatrix} 303 \\ -166 \end{pmatrix}, \begin{pmatrix} -137 \\ 27 \end{pmatrix}, \begin{pmatrix} 351 \\ 112 \end{pmatrix}, \begin{pmatrix} 11 \\ 377 \end{pmatrix}, \begin{pmatrix} -324 \\ 258 \end{pmatrix}, \begin{pmatrix} 127 \\ -43 \end{pmatrix}, \begin{pmatrix} -330 \\ -117 \end{pmatrix},$$

see Fig. 2a. The blue circle visualizes the point $\mathbf{c}(0)$. The polar parameterization (3) by line segments is depicted in Fig. 2b. It is not regular, since the domain is not star-shaped with respect to the origin. In fact, the kernel of the domain is empty and thus the domain is not star-shaped.

Next, we consider the circular arcs obtained by choosing the quasi-periodic function

$$\varphi(t) = 2\pi t - \frac{8}{5}.$$

The resulting parameterization is visualized in Figure 2c. Again it is not regular, since the arcs are not confined to the domain and even intersect each other.

Finally we choose another quasi-periodic function $\varphi(t)$, which will be presented later, and obtain the arc fibration shown in Figure 2d. \diamond

4. Regularity conditions

We investigate conditions that guarantee the regularity of the parameterization by circular arcs. The determinant of the Jacobian matrix of (4) evaluates to

$$D(s, t) = \frac{s((1-s)(x(t)^2 + y(t)^2)^2 \varphi'(t) + sD(1, t))}{(s^2 + 2s(1-s)(x(t) \cos \varphi(t) + y(t) \sin \varphi(t)) + (1-s)^2(x(t)^2 + y(t)^2))^2}, \quad (8)$$

where

$$D(1, t) = (x(t)^2 + y(t)^2) \sqrt{x'(t)^2 + y'(t)^2} \langle \mathbf{u}(t), \mathbf{v}(t) \rangle. \quad (9)$$

The vector $\mathbf{v}(t) = (\cos \varphi(t), \sin \varphi(t))$ denotes the tangent vector at $s = 0$, while

$$\mathbf{u}(t) = \frac{1}{(x(t)^2 + y(t)^2) \sqrt{x'(t)^2 + y'(t)^2}} \begin{pmatrix} (x(t)^2 - y(t)^2)y'(t) - 2x(t)y(t)x'(t) \\ (x(t)^2 - y(t)^2)x'(t) + 2x(t)y(t)y'(t) \end{pmatrix}$$

¹We use $\text{Arg } z$ for the principal value, while $\arg z = \text{Arg } z + 2\pi\mathbb{Z}$ denotes the set of all equivalent angles.

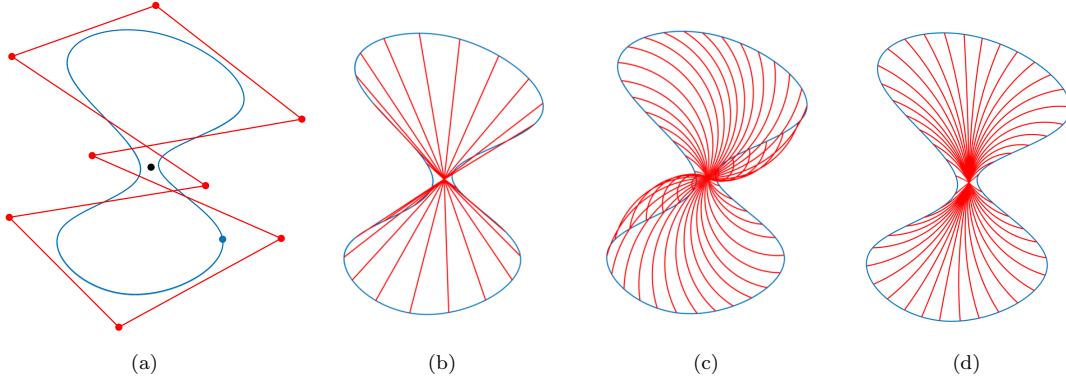


Figure 2: A hourglass-shaped planar domain (a) and polar parameterizations by line segments (b) and circular arcs (c,d). The latter one is an arc fibration.

is obtained by reflecting the curve's unit normal

$$\mathbf{n}(t) = \frac{1}{\sqrt{x'(t)^2 + y'(t)^2}} \begin{pmatrix} -y'(t) \\ x'(t) \end{pmatrix}$$

at the bisector of the origin and $\mathbf{c}(t)$. The reflected unit normal can be represented by smooth arithmetic quasiperiodic function $\psi(t)$ with period 1 and constant 2π , satisfying

$$\begin{pmatrix} \cos \psi(t) \\ \sin \psi(t) \end{pmatrix} = \mathbf{u}(t). \quad (10)$$

In other words, the function $\psi(t)$ fulfills

$$\psi(t) \in \arg((x(t)^2 - y(t)^2)(y'(t) + ix'(t)) - 2x(t)y(t)(x'(t) - iy'(t))) \quad (11)$$

for all t . Clearly, there are countably many possibilities to choose the function $\psi(t)$. We select the one that attains the principal value for $t = 0$, i.e.,

$$\psi(0) = \text{Arg}((x(0)^2 - y(0)^2)(y'(0) + ix'(0)) - 2x(0)y(0)(x'(0) - iy'(0))) \in (-\pi, \pi].$$

In addition, we define the auxiliary functions

$$\varphi_{\min}(t) = \psi(t) - \frac{\pi}{2} \quad \text{and} \quad \varphi_{\max}(t) = \psi(t) + \frac{\pi}{2}.$$

We analyze the regularity of the parameterizations along the domain boundary, i.e., for $s = 1$:

Lemma 2. *The determinant of the Jacobian matrix satisfies $D(1, t) > 0$ if and only if the smooth quasiperiodic function $\varphi(t)$ with period 1 and constant 2π satisfies*

$$\varphi_{\min}(t) + 2k\pi < \varphi(t) < \varphi_{\max}(t) + 2k\pi \quad \forall t, \quad (12)$$

for some integer k .

Proof. The definitions (5) and (10) imply

$$\langle \mathbf{u}(t), \mathbf{v}(t) \rangle = \cos(\varphi(t) - \psi(t)).$$

The claimed result then follows from (9). □

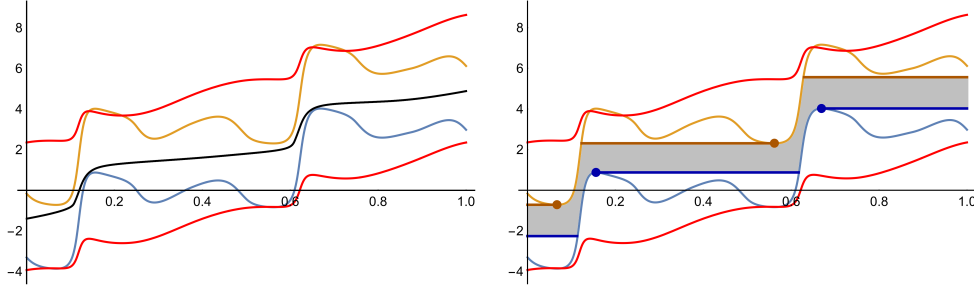


Figure 3: Left: The graphs of $\varphi(t)$ (black) and of the associated auxiliary functions $\varphi_{\text{anti}}(t)$, $\varphi_{\text{max}}(t)$ and $\varphi_{\text{min}}(t)$ (shown in red, orange and blue, respectively) for the arc fibration shown in Fig. 2d. Right: The reduced φ -channel.

The previous result can be extended to provide regularity conditions for the entire polar parameterization, thereby ensuring that it becomes an arc fibration:

Theorem 3. Consider a smooth quasiperiodic function $\varphi(t)$ with period 1 and constant 2π and the polar parameterization (4) defined by it. This polar parameterization is an arc fibration if and only if the function $\varphi(t)$ fulfills the conditions (i)-(iii) below for all $t \in \mathbb{R}$:

- (i) It satisfies the inequalities (12) of Lemma 2,
- (ii) it is strictly increasing, $\varphi'(t) > 0$, and
- (iii) the vectors $\mathbf{v}(t) = (\cos \varphi(t), \sin \varphi(t))$ and $\mathbf{c}(t)$ are not anti-parallel, see (7).

Proof. We analyze the sign of the Jacobian determinant (8), which depends on the function $\varphi(t)$ and on its derivative. On the one hand, Lemma 2 together with $\varphi' > 0$ imply the positivity of the numerator, since all the terms are positive for all $s \in (0, 1]$. The denominator, which is simply the square of the denominator in (4), is positive as well, as observed already in (6) and (7). On the other hand, the determinant takes negative values or is undefined if one of the three conditions is violated. \square

In order to analyze condition (iii), we introduce another auxiliary function $\varphi_{\text{anti}}(t)$, which captures the effect of antiparallel vectors $\mathbf{u}(t)$ and $\mathbf{v}(t)$. More precisely, the function satisfies

$$\varphi_{\text{anti}}(t) \in \arg(-(x(t) + iy(t))) \quad \forall t \quad \text{and} \quad \varphi_{\text{anti}}(0) = \text{Arg}(-(x(0) + iy(0))). \quad (13)$$

Example 2 (Hourglass, continued). We consider again the hourglass shape of Example 1. The plot on the left-hand side of Fig. 3 shows the auxiliary functions $\varphi_{\text{anti}}(t)$, $\varphi_{\text{max}}(t)$ and $\varphi_{\text{min}}(t)$. In addition, we plotted the function $\varphi_{\text{anti}}(t) - 2\pi$ (also in red), in order to take the ambiguity of \arg into account. In order to find a regular arc fibration, we choose a function $\varphi(t)$ (black) that satisfies the conditions of the theorem: Its graph is contained in the channel bounded by $\varphi_{\text{min}}(t)$ and $\varphi_{\text{max}}(t)$, it is strictly increasing, and it does not intersect the red curves. This function defines the arc fibration, which was shown in Fig. 2d. The function $\varphi(t)$ is a quasiperiodic cubic spline with period 1 and constant 2π , defined by 16 polynomial segments in $[0, 1]$. The spline coefficients were chosen manually. \diamond

The final result of this section will be useful for the computation of arc fibrations.

Lemma 4. The auxiliary function $\varphi_{\text{anti}}(t)$ is strictly decreasing whenever

$$\varphi_{\text{min}}(t) < \varphi_{\text{anti}}(t) + 2k\pi < \varphi_{\text{max}}(t) \quad (14)$$

for some integer k .

Proof. A short computation confirms that

$$\varphi'_{\text{anti}}(t) = \frac{x(t)y'(t) - y(t)x'(t)}{x(t)^2 + y(t)^2} = -\frac{\sqrt{x'(t)^2 + y'(t)^2}}{\sqrt{x(t)^2 + y(t)^2}} \left\langle \begin{pmatrix} x(t) \\ y(t) \end{pmatrix}, \mathbf{u}(t) \right\rangle. \quad (15)$$

The inner product on the right hand side is positive if and only if (14) holds. \square

5. Computation of Arc Fibrations

We present an algorithm that can be used to decide whether an arc fibration exists for a given domain boundary \mathbf{c} . It also shows how to find any available arc fibration.

The two quasiperiodic functions $\varphi_{\min}(t)$ and $\varphi_{\max}(t)$ define the φ -channel

$$C = \{(\xi, \eta) \in \mathbb{R}^2 : \varphi_{\min}(\xi) < \eta < \varphi_{\max}(\xi)\}, \quad (16)$$

which is again quasiperiodic in the sense that it satisfies $C = C + (1, 2\pi)$. The graph of any function $\varphi(t)$ defining an arc fibration is contained in C . Since we are only interested in strictly increasing functions, we define the *reduced* φ -channel

$$\hat{C} = \{(\xi, \eta) : \hat{\varphi}_{\min}(\xi) < \eta < \hat{\varphi}_{\max}(\xi)\}, \quad (17)$$

with the help of the two monotonically increasing functions

$$\hat{\varphi}_{\min}(t) = \max_{\tau \leq t} \varphi_{\min}(\tau) \quad \text{and} \quad \hat{\varphi}_{\max}(t) = \min_{\tau \geq t} \varphi_{\max}(\tau).$$

The reduced channel is formed by the graphs of all strictly increasing functions that are contained in C . Graphically, the process of creating \hat{C} from C can be seen as the elimination of all ‘‘pockets’’ of the upper and lower boundary, respectively (see Fig. 3, right).

According to Theorem 3, a valid arc fibration corresponds to a strictly increasing quasiperiodic function $\varphi(t)$ whose graph is contained in \hat{C} . Clearly, such functions exist only if \hat{C} is connected, i.e., only if

$$\hat{\varphi}_{\min}(t) < \hat{\varphi}_{\max}(t) \quad (18)$$

holds for all $t \in \mathbb{R}$. In addition, its graph must not intersect the graph of $\varphi_{\text{anti}}(t)$. We show that the latter graph does not intersect the reduced φ -channel if (18) is satisfied.

Lemma 5. *The reduced φ -channel does not contain any point of the graph of the auxiliary function $\varphi_{\text{anti}}(t)$ if it is connected.*

Proof. We prove this fact by contradiction. Assume there exists a $t_0 \in [0, 1)$ such that $(t_0, \varphi_{\text{anti}}(t_0)) \in \hat{C}$, or, equivalently,

$$\hat{\varphi}_{\min}(t_0) < \varphi_{\text{anti}}(t_0) < \hat{\varphi}_{\max}(t_0).$$

First, we generate two C^1 -smooth monotonic spline approximations $\tilde{\varphi}_{\min}$ and $\tilde{\varphi}_{\max}$ of $\hat{\varphi}_{\min}$ and $\hat{\varphi}_{\max}$, respectively, which satisfy

$$\tilde{\varphi}_{\min}(t_0) < \varphi_{\text{anti}}(t_0) < \tilde{\varphi}_{\max}(t_0) \quad \text{and} \quad \hat{\varphi}_{\min}(t) \leq \tilde{\varphi}_{\min}(t) < \tilde{\varphi}_{\max}(t) \leq \hat{\varphi}_{\max}(t) \quad \forall t \in \mathbb{R}. \quad (19)$$

The approximation of the lower bound is the quadratic spline function

$$\tilde{\varphi}_{\min}(t) = \sum_{i \in \mathbb{Z}} N_i^2(t) \hat{\varphi}_{\min}(\xi_i),$$

where the B-splines N_i^2 are defined with respect to the bi-infinite uniform knot vector $\frac{1}{K}\mathbb{Z}$ and the ξ_i denote the associated Greville abscissas. This approximation preserves the monotonicity since the control points of the spline function are placed on the monotonic function $\hat{\varphi}_{\min}(t)$, thus forming a monotonic control polygon. It also converges to that function as the knot density K increases, hence it satisfies (19) if K is large enough. An analogous construction is used to generate the approximate upper bound $\tilde{\varphi}_{\max}(t)$. Both approximations are again quasiperiodic.

Now, let

$$\lambda = \frac{\varphi_{\text{anti}}(t_0) - \tilde{\varphi}_{\min}(t_0)}{\tilde{\varphi}_{\max}(t_0) - \tilde{\varphi}_{\min}(t_0)}. \quad (20)$$

We define the function

$$\sigma(t) = \lambda \tilde{\varphi}_{\max}(t) + (1 - \lambda) \tilde{\varphi}_{\min}(t) \quad (21)$$

that satisfies $\sigma(t_0) = \varphi_{\text{anti}}(t_0)$. Moreover, it is monotonically increasing since it is a convex combination of two monotonic functions. Consider the difference $\delta(t) = \varphi_{\text{anti}}(t) - \sigma(t)$. The auxiliary function $\varphi_{\text{anti}}(t)$ is strictly decreasing in a certain vicinity of t_0 , according to Lemma 4. Thus, the derivative $\delta'(t_0)$ is negative, and so is $\delta'(t_0 + 1)$, due to the periodicity. Moreover, both t_0 and $t_0 + 1$ are roots of $\delta(t)$. Consequently, there exists $\varepsilon > 0$ such that δ takes negative values on the interval $(t_0, t_0 + \varepsilon)$, and positive values on $(t_0 + 1 - \varepsilon, t_0 + 1)$. Hence, there exists at least one root between t_0 and $t_0 + 1$. Let t_1 be the smallest such root.

We have

$$\tilde{\varphi}_{\min}(t_1) < \sigma(t_1) = \varphi_{\text{anti}}(t_1) < \tilde{\varphi}_{\max}(t_1) \quad (22)$$

since the approximate reduced φ -channel is connected and $\delta(t_1) = 0$. We use Lemma 4 to confirm that the derivative $\delta'(t)$ is negative at t_1 , hence there exists $\tilde{\varepsilon} > 0$ such that δ takes positive values on the interval $(t_1 - \tilde{\varepsilon}, t_1)$. Consequently, the difference function possesses at least one root between t_0 and t_1 , thereby contradicting the assumption that t_1 was the smallest root between t_0 and $t_0 + 1$. \square

According to this Lemma, it suffices to construct a function $\varphi(t)$ by taking into account the first two conditions of Theorem 3. This is done by executing the following algorithm:

1. Find the functions $\varphi_{\min}(t)$ and $\varphi_{\max}(t)$.
2. Eliminate the pockets by evaluating the functions $\hat{\varphi}_{\min}(t)$ and $\hat{\varphi}_{\max}(t)$ that define the reduced φ -channel.
3. If the reduced φ -channel is connected, i.e., if $\hat{\varphi}_{\min}(t) < \hat{\varphi}_{\max}(t)$ holds for all $t \in \mathbb{R}$, then select a quasiperiodic function $\varphi(t)$ with period 1 and constant 2π , which is strictly increasing and contained in the channel.

In our examples, the function $\varphi(t)$ was chosen as a quasiperiodic spline function, which was created manually. The construction of monotonic spline functions by interpolation or approximation is well studied (see [Dierckx, 1995](#); [Zhu, 2018](#), and the references cited therein). A simple construction is sketched in the remark below.

Remark 2. The third step of the algorithm described above can be realized by the following procedure. First, we choose a constant $\varepsilon \leq \frac{1}{2} \min_{t \in \mathbb{R}} |\hat{\varphi}_{\max}(t) - \hat{\varphi}_{\min}(t)|$ and define the upper and lower bounds with reduced slope,

$$\varphi_{\min}^\varepsilon(t) = \varphi_{\min}(t) - \varepsilon t, \quad \text{and} \quad \varphi_{\max}^\varepsilon(t) = \varphi_{\max}(t) - \varepsilon t.$$

Second, we eliminate the pockets in the associated channel by defining

$$\hat{\varphi}_{\min}^\varepsilon(t) = \max_{\tau \leq t} \varphi_{\min}^\varepsilon(\tau) \quad \text{and} \quad \hat{\varphi}_{\max}^\varepsilon(t) = \min_{\tau \geq t} \varphi_{\max}^\varepsilon(\tau).$$

The choice of ε ensures that the channel defined by these two functions is still connected. Consequently, the average

$$\varphi^\varepsilon(t) = \frac{1}{2}(\hat{\varphi}_{\min}^\varepsilon(t) + \hat{\varphi}_{\max}^\varepsilon(t))$$

is contained in that channel. Finally we eliminate the effect of the reduced slope and create a monotonic C^1 -smooth spline function

$$\varphi(t) = \sum_{i \in \mathbb{Z}} N_i^2(t)(\hat{\varphi}^\varepsilon(\xi_i) + \varepsilon \xi_i),$$

by considering again the knots and B-splines N_i (with associated Greville abscissas ξ_i) that were used in the proof of Lemma 5. \diamond

We present two examples of arc fibrations that were created by the algorithm.

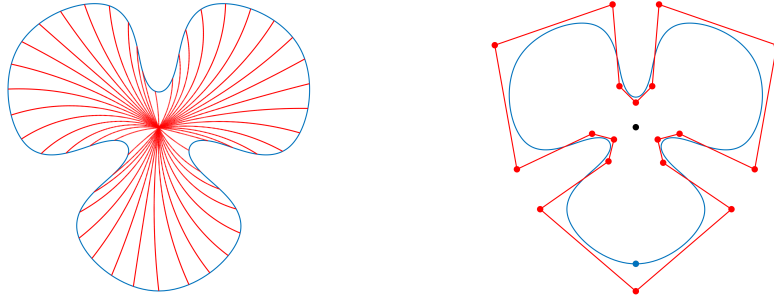


Figure 4: Arc fibration (left) of a clover-shaped planar domain (right) defined by a cubic spline with 18 control points.

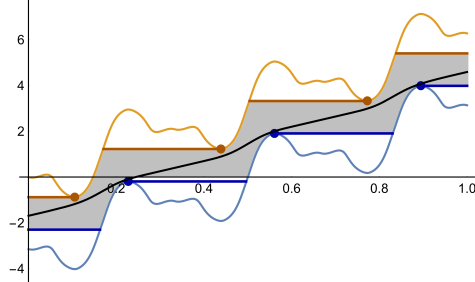


Figure 5: Reduced φ -channel and the function φ that defines the arc fibration shown in Fig. 4.

Example 3 (Clover). We consider a clover-shaped planar domain, which is bounded by a periodic cubic spline curve $\mathbf{c}(t)$ with uniform knots and 18 control points, see Fig. 4 (right). The reduced φ -channel (shown in Fig. 5) is connected. We create a strictly increasing quasiperiodic cubic spline (black curve), defined by 13 polynomial segments, which is contained in the channel. The resulting arc fibration is also shown in Fig. 4 (left). \diamond

Example 4 (Seal). We consider a planar domain in the shape of a seal, which is bounded by a periodic cubic spline curve $\mathbf{c}(t)$ with uniform knots and 24 control points, see Fig. 6 (right). The function $\varphi(t)$ is chosen as a quasiperiodic cubic spline with period 1 and constant 2π , defined by 11 polynomial segments in $[0, 1]$. As we can see in Fig. 7, the chosen function $\varphi(t)$ (shown in black) is contained within the reduced φ -channel and is strictly increasing. Consequently, it defines an arc fibration, see Fig. 6, left. \diamond

6. Arc Fibration Kernel

So far, we studied parameterizations (4) defined by circular arcs that connect the *origin* of the coordinate system with points on the domain's boundary. Consequently, the procedure described in the previous section allows to decide whether an arc fibration of this form exists. Clearly, the answer and the resulting arc fibration then depends on the choice of the origin of the coordinate system.

Now, given a planar domain, we consider parameterizations with respect to an arbitrarily chosen origin of the coordinate system. We will refer to the origin as the *center* of the parameterization.

Definition 6. We say that a center is *valid* if an associated arc fibration exists. The valid points form the *arc fibration kernel*.

We start the discussion by a simple example:

Example 5 (Hourglass). We consider the reduced φ -channels of the hourglass-shaped domain for the three centers shown in Fig. 8. The first channel is connected, the third one disconnected, and the second represents the transition case. Consequently, the first center belongs to the arc fibration kernel, and the second one is located on its boundary. \diamond

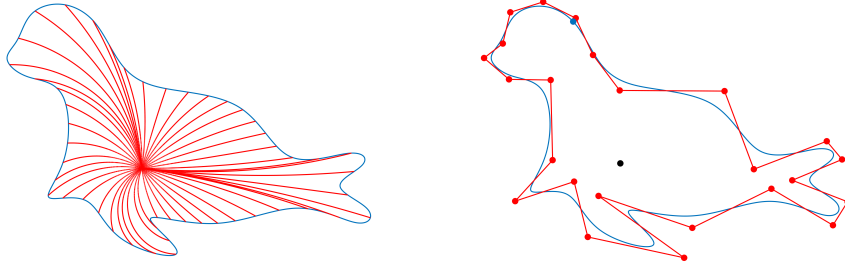


Figure 6: Arc fibration (left) of a seal-shaped planar domain (right) defined by a cubic spline with 24 control points.

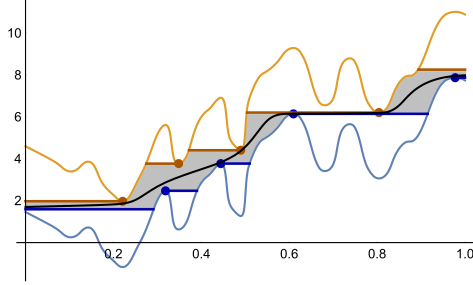


Figure 7: Reduced φ -channel and the function φ that defines the arc fibration shown in Fig. 6.

We conclude that the boundary of the arc fibration kernel is characterized by the fact *that the boundary curves of the associated φ -channel share a horizontal tangent*. As a first step, we analyze these tangents, which correspond to stationary points of $\psi(t)$ defined in (10).

Lemma 7. *The function $\psi(t)$ possesses a stationary point at t_0 , i.e.*

$$\psi'(t_0) = \varphi'_{\min}(t_0) = \varphi'_{\max}(t_0) = 0, \quad (23)$$

if and only if the osculating circle of the boundary curve at $c(t_0)$ passes through the center.

Proof. Without loss of generality, we assume that the boundary curve \mathbf{c} is given by an arc-length parameterization. Consequently, its unit tangent vector satisfies $\mathbf{t} = \mathbf{c}'$. Recall that the center (i.e., the origin of the coordinate system) is contained in the interior of the domain, hence $\langle \mathbf{c}, \mathbf{c} \rangle \neq 0$.

First we examine the case of nonzero curvature $\kappa \neq 0$. We consider the reflected normal vector

$$\mathbf{u} = \mathbf{n} - 2 \frac{\langle \mathbf{c}, \mathbf{n} \rangle}{\langle \mathbf{c}, \mathbf{c} \rangle} \mathbf{c}, \quad (24)$$

which defines the function ψ . On the one hand, we use the Frenet formulas to confirm that its derivative satisfies

$$\mathbf{u}' = \left(\kappa + 2 \frac{\langle \mathbf{c}, \mathbf{n} \rangle}{\langle \mathbf{c}, \mathbf{c} \rangle} \right) (-\mathbf{t} + 2 \frac{\langle \mathbf{c}, \mathbf{t} \rangle}{\langle \mathbf{c}, \mathbf{c} \rangle} \mathbf{c}). \quad (25)$$

A short computation confirms that the second factor, which is a vector, has norm 1. On the other hand, the osculating circle passes through the center iff

$$0 = \left\langle \mathbf{c} + \frac{1}{\kappa} \mathbf{n}, \mathbf{c} + \frac{1}{\kappa} \mathbf{n} \right\rangle - \frac{1}{\kappa^2} = \frac{\langle \mathbf{c}, \mathbf{c} \rangle}{\kappa} \left(\kappa + 2 \frac{\langle \mathbf{c}, \mathbf{n} \rangle}{\langle \mathbf{c}, \mathbf{c} \rangle} \right). \quad (26)$$

Clearly, the latter equation is satisfied if and only if $\mathbf{u}' = 0$.

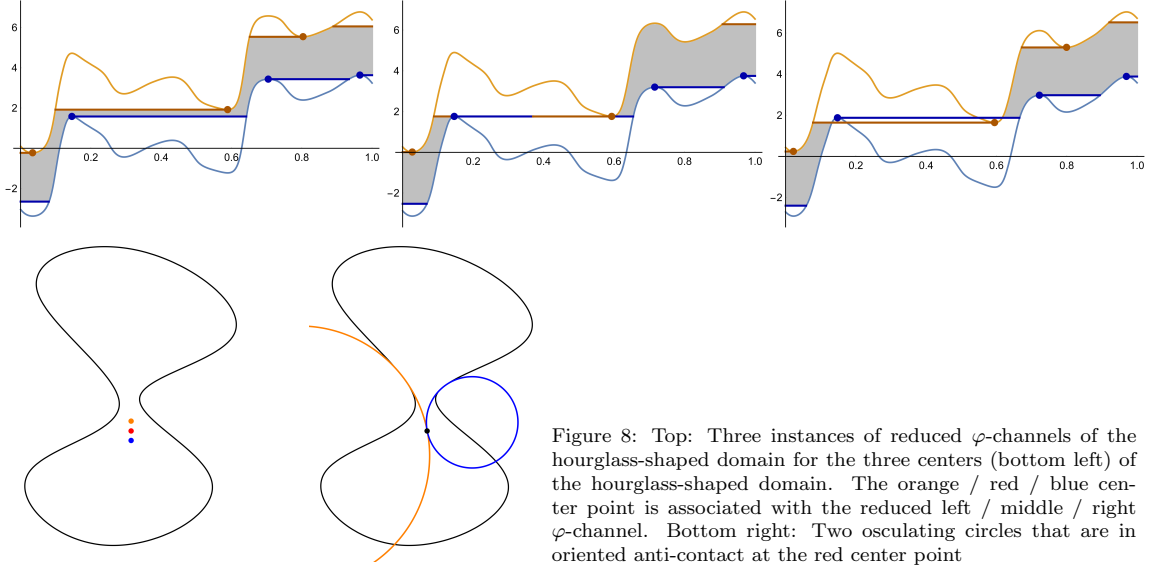


Figure 8: Top: Three instances of reduced φ -channels of the hourglass-shaped domain for the three centers (bottom left) of the hourglass-shaped domain. The orange / red / blue center point is associated with the reduced left / middle / right φ -channel. Bottom right: Two osculating circles that are in oriented anti-contact at the red center point

Second we consider inflection points, $\kappa = 0$, where

$$\mathbf{u}' = 2 \frac{\langle \mathbf{c}, \mathbf{n} \rangle}{\langle \mathbf{c}, \mathbf{c} \rangle} \left(-\mathbf{t} + 2 \frac{\langle \mathbf{c}, \mathbf{t} \rangle}{\langle \mathbf{c}, \mathbf{c} \rangle} \mathbf{c} \right). \quad (27)$$

The inflection tangent, which represents the osculating circle in this case, intersects the center iff $0 = \langle \mathbf{c}, \mathbf{n} \rangle$, thereby completing the proof. \square

Now we combine this result with the previously derived characterization of boundary points of the arc fibration kernel.

Consider a horizontal tangent that is shared by the two boundary curves of the associated φ -channel. It touches the boundaries in two distinct points with abscissas t_1 and t_2 . Thus we have

$$\varphi'_{\min}(t_1) = 0, \quad \varphi'_{\max}(t_2) = 0 \quad (28)$$

and

$$\varphi_{\min}(t_1) = \varphi_{\max}(t_2). \quad (29)$$

The two equations (28) imply that the two osculating circles at $\mathbf{c}(t_1)$ and $\mathbf{c}(t_2)$ pass through the center, due to the previous lemma. Moreover, the circular arc $p(s, t_1)$ defined by the polar parameterization (4) with $\varphi(t) = \varphi_{\min}(t)$ is a segment of the osculating circle at t_1 , since they share two points (the center and $\mathbf{c}(t_1)$) and a tangent (the tangent at $\mathbf{c}(t_1)$). Similarly, the circular arc $p(s, t_2)$ defined by the polar parameterization (4) with $\varphi(t) = \varphi_{\max}(t)$ is a segment of the osculating circle at t_2 .

Combining this observation with (29) confirms that the two osculating circles at $\mathbf{c}(t_1)$ and $\mathbf{c}(t_2)$ are in tangential contact at the center. A closer analysis reveals that they touch each other with opposite orientation, where their orientation is determined by $\mathbf{c}(t)$. We say that the circles are in *oriented anti-contact*. An example is shown in Fig. 8 (top right), where the blue and orange circle are both oriented clockwise.

This fact motivates us to introduce another notion:

Definition 8. The points where two osculating circles of the domain boundary touch each other with opposite orientation will be denoted as the *Osculating Circles oriented Anti-Contact (OCAC) points*.

Each OCAC point is determined by two points $\mathbf{c}(t_1)$ and $\mathbf{c}(t_2)$ that generate the two touching oppositely oriented osculating circles. The anti-contact condition leads to the equation

$$\kappa(t_1)\kappa(t_2)\|\mathbf{c}(t_1) - \mathbf{c}(t_2)\|^2 + 2\kappa(t_1)\langle \mathbf{c}(t_2) - \mathbf{c}(t_1), \mathbf{n}(t_2) \rangle + 2\kappa(t_2)\langle \mathbf{c}(t_1) - \mathbf{c}(t_2), \mathbf{n}(t_1) \rangle = 2\langle \mathbf{n}(t_1), \mathbf{n}(t_2) \rangle + 2 \quad (30)$$

For any pair (t_1, t_2) satisfying this condition, we obtain the associated point

$$\mathbf{q}(t_1, t_2) = \frac{1}{\kappa(t_1) + \kappa(t_2)} (\kappa(t_1)\mathbf{c}(t_1) + \mathbf{n}(t_1) + \kappa(t_2)\mathbf{c}(t_2) + \mathbf{n}(t_2)) \quad (31)$$

on the OCAC curve.

Finally we state a characterization of the arc fibration kernel's boundary:

Theorem 9. *The boundary of the arc fibration kernel consists of domain boundary points and OCAC points.*

Proof. A point in the interior of the domain belongs to the boundary of the arc fibration kernel if the associated φ -channel shrinks to a line segment for some interval of the t axis, see Fig. 5. This implies the existence of a common horizontal tangent of $\varphi_{\min}(t)$ and $\varphi_{\max}(t)$, and thus the point satisfies the criteria of Definition 8. \square

Example 6. We used MapleTM to compute the arc fibration kernel of the symmetric hourglass planar shape shown in Fig. 9 (top right, black curve). The boundary is represented by a trigonometric polynomial curve of order 3. The parameter values of the OCAC points, which are defined by Eq. (30), form an curve in the (t_1, t_2) -plane, which is visualized in the top left plot. Note that this curve is not only symmetric but also 1-periodic with respect to both coordinate axes.

Transforming this curve into the physical domain via (31) gives the OCAC curves, which are shown in green and blue. One of them (shown in blue) forms the boundary of the arc fibration kernel, which is located in the central part of the domain. This can be confirmed by analyzing the φ -channels of sample points within the domain. It suffices to check the φ -channel of one center point for each face of the planar subdivision of the domain that is defined by the OCAC curves (shown in green and blue).

Three instances of points (marked by circles, top right) and associated φ -channels are shown (bottom row). The leftmost (connected) channel corresponds to highest point, which is located within the kernel. The other two channels are associated with the remaining two points that do not belong to the arc fibration kernel. \diamond

In general, the OCAC curve is a superset of the boundary of the arc fibration kernel. More precisely, the points of this curve can be classified into several groups, depending on the signs and the magnitudes of the curvatures at the two corresponding points on the boundary, and on the signs of the curvature derivative. The latter signs specifies whether the osculating circle *enters* or *leaves* the domain². There are six cases if both osculating circles possess the same orientation, which is either positive or negative, see Fig. 10. Only one of them, which is characterized by negative curvatures and different signs of the curvature derivative, may contribute to the boundary of the arc fibration kernel.

The remaining cases – where the curvatures possess opposite signs – can be transformed into to one of these six cases via a suitable Möbius transformation. For instance, a mapping that sends the point marked by ∞ in the bottom left picture of Fig. 10 to the ideal point of the complex plane transforms this case into the fifth case (which was the relevant one for the computation of the arc fibration kernel boundary). Consequently, the above classification can be extended to these situations, since arc fibrations and their kernels are invariant under these transformations.

This observation can be used to filter the OCAC points. Even after applying this filter, however, not all remaining points necessarily contribute to the boundary of the arc fibration kernel. The true boundary can be identified as in Example 6, simply by analyzing a φ -channel for one center in each face of the planar subdivision defined by filtered curve.

The final example compares the flexibility of polar parameterizations by lines and by circular arcs.

²Here we need to assume that the boundary curve is C^3 smooth. Except for curvature extrema, the osculating circle of a curve crosses the curve at the associated point.

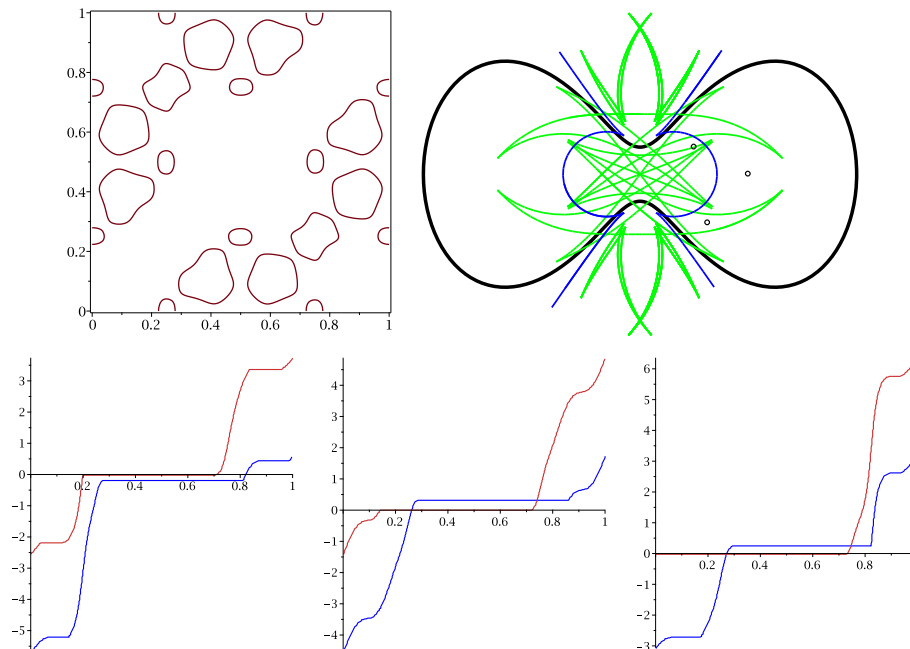


Figure 9: Top row: OCAC curves of a planar domain (bounded by the black curve, right) in the (t_1, t_2) -parameter domain (left) and in the physical domain (right, blue and green curves). The blue curve forms the boundary of the arc fibration kernel. Bottom row: φ -channels associated with three selected center points (marked by circles in the top right picture).

Example 7. Figure 11 compares the kernels and the arc fibration kernels of three hourglass-shaped planar domains, which have been generated by stretching. We start with a domain (left), where both kernels are non-empty. For the second domain (center), the kernel shrinks to a point, while the arc fibration kernel is still quite large. After some further stretching (right), the latter kernel shrinks to a point also. \diamond

7. Conclusion

The notion of arc fibrations forms an interesting generalization of polar parameterizations by line segments. While the latter parameterizations are available for star-shaped domains only, the use of arc fibrations provides additional geometric flexibility. The existence of an arc fibration for a given planar domain can be analyzed by a simple geometry-based algorithm, which also allows to compute it in the affirmative case. The arc fibration kernel, which contains all the feasible center points of a domain, is bounded by the curve of OCAC points and by the domain boundary. Its analysis makes it possible to decide whether a planar domain possesses an arc fibration or not.

It should be noted that arc fibrations and the class of planar domains admitting them are invariant under Möbius transformations that preserve the orientation of the domain's boundary curve. (The interested reader may wish to consult the textbooks of [Hertrich-Jeromin \(2003\)](#) or [Kisil \(2012\)](#) for a detailed introduction to Möbius geometry.) In particular, the OCAC curve is also invariant, since Möbius transformations preserve osculating circles.

Future work will be devoted to more efficient methods for computing the arc fibration kernel. It turns out that this computation becomes much simpler for domains bounded by arc splines, similar to the problem of medial axis computation ([Aichholzer et al., 2009](#)). Arc splines, however, are not C^2 -smooth, hence one

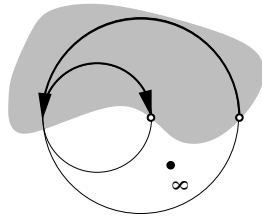
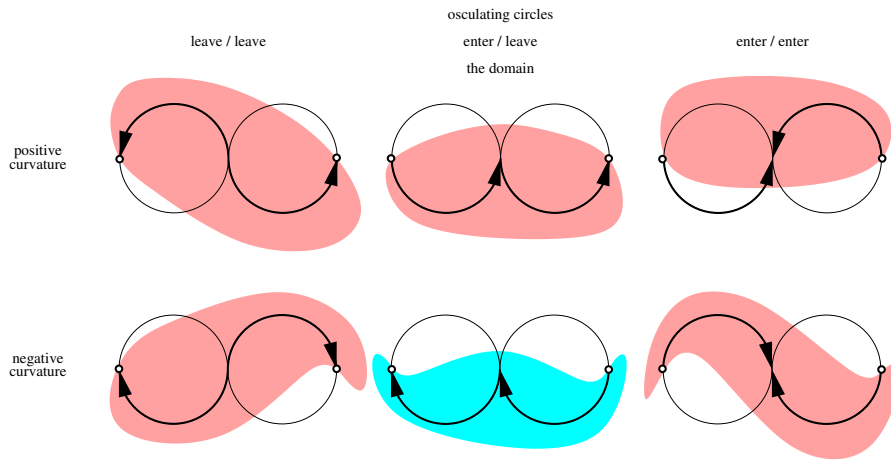


Figure 10: Above: The six cases of OCAC points for curvatures possessing the same sign. Only the situation shown in the second picture of the second row is relevant for the boundary of the arc fibration kernel. Left: Situations with different curvature signs can be transformed to one of these six cases by a suitable Möbius transformation.

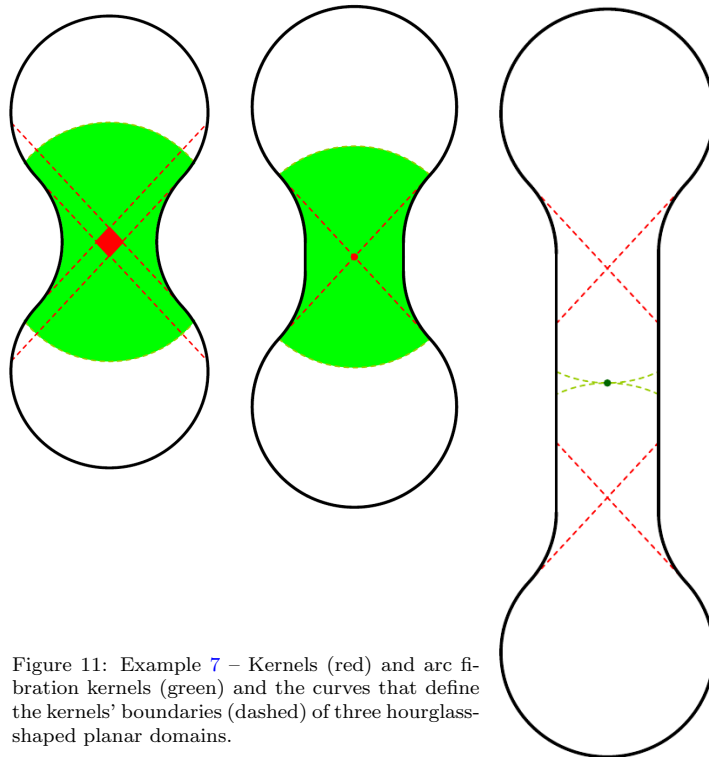


Figure 11: Example 7 – Kernels (red) and arc fibration kernels (green) and the curves that define the kernels' boundaries (dashed) of three hourglass-shaped planar domains.

needs a slightly different analysis, which will be presented in a forthcoming paper (Weiß and Jüttler, 2019). We also plan to explore the generalization to three-dimensional domains.

In addition, it should be interesting to explore fibrations by more general curves, such as low degree Bézier curves. It is well known that any contractible domain possesses a polar parameterization, and Gondegaon and Voruganti (2018) used this observation to create domain parameterizations for isogeometric analysis, while Huynh and Gingold (2015) employed integral curve coordinates to define bijective deformations. Alternatively, one may consider polygons defining piecewise linear foliations (cf. Campen et al., 2016). The restriction to low degree parameter lines may make the simulation computationally more efficient and introduces a natural geometric classification of contractible domains.

Acknowledgment

Supported by the Austrian Science Fund through NFN S117 “Geometry + Simulation”. The authors thank Bastian Weiß for his help.

References

- Aichholzer, O., Aigner, W., Aurenhammer, F., Hackl, T., Jüttler, B., Rabl, M., 2009. Medial axis computation for planar free-form shapes. *Computer-Aided Design* 41, 339–349.
- Aichholzer, O., Aurenhammer, F., Hackl, T., Jüttler, B., Rabl, M., Šír, Z., 2011. Structural and computational advantages of circular boundary representation. *Int. J. Comp. Geom. Appl.* 21, 47–69.
- Avis, D., Toussaint, G., 1981. An efficient algorithm for decomposing a polygon into star-shaped polygons. *Pattern Recognition* 13, 396–398.
- Campen, M., Silva, C.T., Zorin, D., 2016. Bijective maps from simplicial foliations. *ACM Trans. Graphics* 35, Article no. 74.
- Chen, L., Simeon, B., Klinkel, S., 2016. A NURBS based Galerkin approach for the analysis of solids in boundary representation. *Comp. Meth. Appl. Mech. Engrg.* 305, 777–805.
- Dierckx, P., 1995. *Curve and surface fitting with splines*. Oxford University Press.
- Dobkin, D., Souvaine, D., 1990. Computational geometry in a curved world. *Algorithmica* 5, 421–457.
- Elber, G., Johnstone, J., Kim, M.S., Seong, J.K., 2006. The kernel of a freeform surface and its duality with the convex hull of its tangential surface. *Int. J. Shape Modeling* 12, 129–142.
- Elber, G., Sayegh, R., Barequet, G., Martin, R., 2005. Two-dimensional visibility charts for continuous curves, in: *Proc. Int. Conf. Shape Modeling and Applications*, pp. 208–217.
- Gondegaon, S., Voruganti, H., 2018. An efficient parametrization of planar domain for isogeometric analysis using harmonic functions. *J. Braz. Soc. Mech. Sciences Engrg.* 40, Article no. 493.
- Hertrich-Jeromin, U., 2003. Introduction to Möbius differential geometry. volume 300 of *London Math. Soc. Lecture Note Series*. Cambridge University Press.
- Hughes, T., Cottrell, J., Bazilevs, Y., 2005. Isogeometric analysis: CAD, finite elements, NURBS, exact geometry, and mesh refinement. *Comp. Meth. Appl. Mech. Engrg.* 194, 4135–4195.
- Huynh, L., Gingold, Y.I., 2015. Bijective deformations in \mathbb{R}^n via integral curve coordinates. arXiv e-print no. 1505.00073.
- Joshi, S., Rao, Y., Sundar, B.R., Muthuganapathy, R., 2017. On the visibility locations for continuous curves. *Computers and Graphics* 66.
- Kisil, V., 2012. *Geometry of Möbius transformations*. Imperial College Press, London.
- Lee, D., Preparata, F., 1979. An optimal algorithm for finding the kernel of a polygon. *Journal of the ACM* 26, 415–421.
- Natarajan, S., Wang, J., Song, C., Birk, C., 2015. Isogeometric analysis enhanced by the scaled boundary finite element method. *Comp. Meth. Appl. Mech. Engrg.* 283, 733–762.
- O’Rourke, J., Supowit, K., 1983. Some NP-hard polygon decomposition problems. *IEEE Transactions on Information Theory* 29, 181–190.
- Weiß, B., Jüttler, B., 2019. Arc fibrations of planar domains with arc spline boundaries. In preparation.
- Zhu, Y., 2018. C^2 rational quartic/cubic spline interpolant with shape constraints. *Results Math.* 73, Article no. 127.
- Zubė, S., 2006. A circle representation using complex and quaternion numbers. *Liet. Mat. Rink.* 46, 298–310. English translation in *Lithuanian Math. J.* 46(2):246–255, 2006.